inter.noise
HAMBURG 2016

Effects of geometrical nonlinearities on the acoustic black hole effect

V. Denis[1,*], A. Pelat[1], C. Touzé[2] and F. Gautier[1]

[1]Laboratoire d'Acoustique de l'Université du Maine, UMR CNRS 6613, Avenue Olivier Messiaen 72000 Le Mans cedex 9, France
[2]IMSIA, ENSTA ParisTech, CNRS, CEA, EDF, Université Paris-Saclay, 828 bd des Maréchaux, 91762 Palaiseau cedex, France
[*]vivien.denis@univ-lemans.fr

ABSTRACT

The Acoustic Black Hole effect (ABH) is a passive vibration damping technique without added mass based on flexural waves properties in thin structures with variable thickness. The usual implementation on plates is a region where the thickness is reduced with a power law profile, covered with a visco-elastic layer. The inhomogoneity induces a decrease of the wave speed and an increase of the amplitude in the small thickness region, which makes the energy dissipation more efficient due to the absorbing layer. The wave amplitude in the ABH easily reaches the plate thickness and is the origin of geometrical nonlinearities. These nonlinearities can generate coupling between linear beam eigenmodes of the structure and induce energy transfer between low and high frequency regime. This phenomenon may be used to increase the efficiency of the ABH treatment in the low frequency regime where it is usually inefficient. An experimental investigation shows that the ABH termination displays a nonlinear behaviour and allows for modal coupling. A strongly nonlinear regime can also be observed, which is associated with Wave Turbulence. A model of nonlinear ABH beam as von Kármán plate of variable thickness and a modal resolution of the problem confirm the observed effects and gives more insights on these results.

Keywords: Vibration, Damping, Acoustic Black Hole, Nonlinear

1. INTRODUCTION

The control of undesired vibrations is an important concern in many industrial applications. The classical methods for broadband vibration reduction generally involve the use of heavy layers of damping material. These methods are well-known and very efficient but also lead to an added mass that can be prohibitive in the transport industry for example. There is thus a need for damping techniques without added mass, such as the Acoustic Black Hole (ABH) effect [1, 2].

As described by Mironov [3], this effect takes advantage of the flexural wave properties in a plate with inhomogeneous thickness. It can be shown that waves propagating in a beam with thickness $h(x)$

$$h(x) = \epsilon x^m, \quad m \geq 2, \tag{1}$$

slow down without being reflected and that their travel time in the profile tends to infinity if thickness tends to zero. The residual thickness in this "Acoustic Black Hole" profile is however too large to obtain the effect wanted but this can be compensated by adding a thin viscoelastic layer [1]. The reflection coefficient of the extremity is then considerably reduced. Other theoretical works propose a more refined model for the reflection coefficient [2] and demonstrate the increase of the modal overlap [4]. Experimental evidences of the effect are numerous [5–7].

The minimum thickness of the ABH extremity needed to obtain an important damping is very small (few dozens of microns) and the displacement amplitudes at the extremity become large with respect to the thickness. It questions the linearity of the response of the structure. This paper proposes to demonstrate the nonlinear behaviour of a beam with an ABH extremity

and to show that the geometrical nonlinearities have an influence of the damping properties of the ABH. The first part is an experimental observation of an ABH beam. The second part proposes a numerical model to simulate the response of an ABH beam in nonlinear regimes. Finally, the numerical results are presented in the third part.

2. EXPERIMENT

2.1 Setup

The experimental study concerns two aluminium beams : the first is uniform with dimensions 1.3 m $\times$ 20 mm $\times$ 5 mm, the second with dimensions 1.5 m $\times$ 20 mm $\times$ 5 mm, has a Acoustic Black Hole termination of length 0.35 m; the thickness of this extremity decreases quadratically down to 50 μm approximately. A thin damping layer is applied on the ABH extremity (see Fig. 1).

The experimental setup consists in a shaker (LDS V201), an amplifier (LDS PA25E), a force sensor (PCF 208C03), an accelerometer (PCB 352C29) and an acquisition card (NI-USB4431). It is driven by a Labview interface and the results are exported and treated with MATLAB. The beam to be measured is vertically suspended and excited at midpoint with the shaker. The accelerometer is placed at an arbitrary location on the beam.

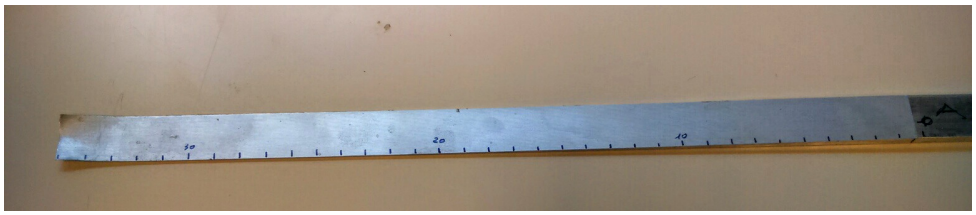

Figure 1: Extremity of the ABH beam. The length of the variable thickness region is 35 cm.

2.2 Filtered white noise excitation

The beams are excited with a filtered white noise excitation on the 200-300 Hz range, for several amplitudes. The power density spectrums of the responses are displayed on Fig. 2. Fig. 2(a) shows that the uniform beam has a linear behaviour since the power is concentrated in the excitation range, except for few artefacts that may come from the setup. On the contrary, in the ABH case (see Fig. 2(b)), the power largely leaks outside the excitation range for high levels of excitation. This energy transfer can be attributed to a nonlinear behaviour. It is particularly interesting since it could be used to transfer energy from low to high frequency domain, that is inherently more damped, in order to increase the efficiency of the ABH treatment in low frequency. However, no reduction of the vibratory levels with the increase of amplitude can be observed in this experiment.

3. MODEL OF NONLINEAR ACOUSTIC BLACK HOLE

3.1 A von Kármán plate model

The ABH beam is modelled as a nonlinear von Kármán plate [8, 9] with variable thickness. The geometry of the plate is described on Fig. 3. The thickness in the ABH region is given by:

$$h(x) = h_t + (h_0 - h_t)\frac{(x - l_{\text{add}})^m}{l_{\text{ABH}}^m}, \tag{2}$$

where h_0 is the thickness of the plate thickness in the uniform region, h_t is the minimum thickness of the plate, m is the exponent of the ABH profile, l_{ABH} is the length of the region of

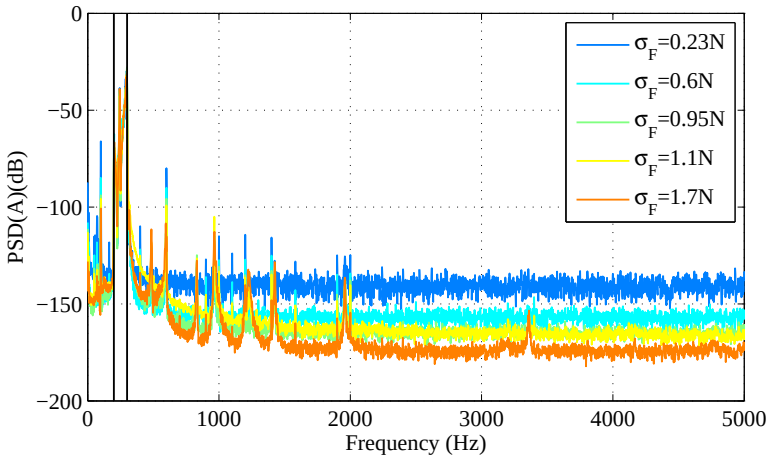

(a)

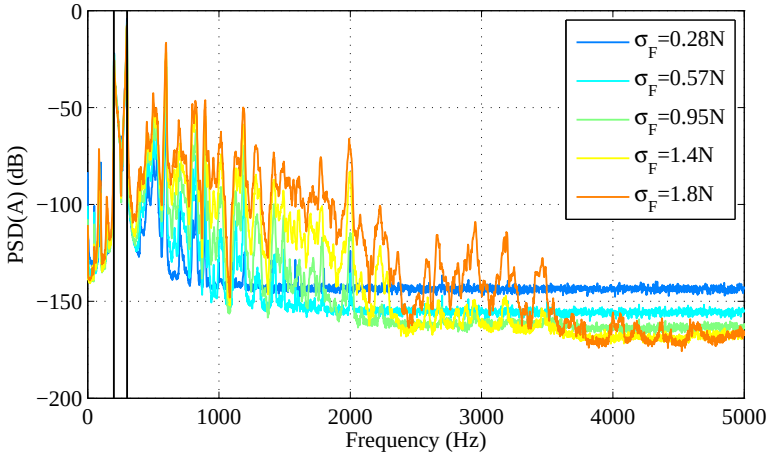

(b)

Figure 2: Power density spectrum of the response to a filtered white noise (200-300 Hz) excitation, normalized by the standard deviation of the force for (a) uniform beam and (b) ABH beam. σ_F denotes the standard deviation of the exciting force.

variable thickness and l_{add} is the length of the extension of small constant thickness.

The equation of motion for the transverse displacement w then writes, following the developments proposed in [10, 11]:

$$\rho h(\mathbf{x})\ddot{w} + \Delta(D(\mathbf{x})\Delta w) - (1-\nu)L(D(\mathbf{x}), w) = p + L(w, F) \tag{3}$$

where the Airy stress function F respects:

$$\Delta(\frac{1}{Eh(\mathbf{x})}\Delta F) - (1+\nu)L(\frac{1}{Eh(\mathbf{x})}, F) = -\frac{1}{2}L(w, w) \tag{4}$$

and where p is the exciting force per unit surface, E is the Young modulus, ν is the Poisson ration, h is the thickness, $D(\mathbf{x}) = Eh(\mathbf{x})^3/12(1-\nu^2)$ is the bending stiffness, ρ is the mass density and $L(f, g)$ is the Monge-Ampère bilinear operator which reads, in cartesian coordinates:

$$L(f, g) = f_{xx}g_{yy} + f_{yy}g_{xx} - 2f_{xy}g_{xy}, \tag{5}$$

where f_{xx} denotes the second derivative of f with respect to x.

In the case of a plate with free edges, the boundary conditions writes, on an edge with normal

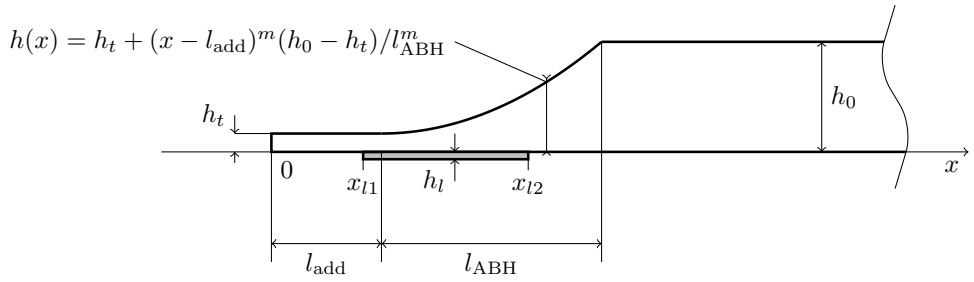

Figure 3: Schematic view of the ABH plate thickness profile. h_0 is the thickness of the plate thickness in the uniform region, h_t is the minimum thickness of the plate, m is the exponent of the ABH profile, l_{ABH} is the length of the region of variable thickness and l_{add} is the length of the extension of small constant thickness. The damping layer stands between abscissas x_{l1} and x_{l2}.

n and tangent τ [4, 11]:

$$-\frac{\partial}{\partial n}\left(D\left(\frac{\partial^2 w}{\partial n^2}+\nu\frac{\partial^2 w}{\partial \tau^2}\right)\right)-2(1-\nu)\frac{\partial}{\partial \tau}\left(D\frac{\partial^2 w}{\partial n \partial \tau}\right)=0, \tag{6}$$

$$\frac{\partial^2 w}{\partial \tau^2}+\nu\frac{\partial^2 w}{\partial n^2}=0, \tag{7}$$

$$F=\frac{\partial F}{\partial n}=0. \tag{8}$$

3.2 Modal projection

A modal projection method [12] is used for solving this model. Eqs. (3) and (4) are projected on the linear eigenmodes of the structure. The conservative and linear associated problems read:

$$\rho h(\mathbf{x})\ddot{w}+\Delta(D(\mathbf{x})\Delta w)-(1-\nu)L(D(\mathbf{x}),w)=0 \tag{9}$$

and

$$\Delta(\frac{1}{Eh(\mathbf{x})}\Delta F)-(1+\nu)L(\frac{1}{Eh(\mathbf{x})},F)=\zeta^4 F \tag{10}$$

to which are added the boundary conditions (6-7). These are eigenvalue problems with solutions $(\omega_k, \Phi_k(\mathbf{x}))$ and $(\zeta_n, \Psi_n(\mathbf{x}))$, respectively. The displacement and the Airy stress function are expressed as:

$$w(\mathbf{x},t)=\sum_{k=1}^{N_\Phi}\Phi_k(\mathbf{x})q_k(t), \tag{11}$$

and

$$F(\mathbf{x},t)=\sum_{n=1}^{N_\Psi}\Psi_n(\mathbf{x})\beta_n(t). \tag{12}$$

It is emphasized that the modes are normalized such that their scalar product is unitary:

$$<\Phi_k,\Phi_k>=1. \tag{13}$$

The projection on the linear modes gives the formulation (14-15) quadratic in (q,β), which writes:

$$\beta_p(t)=-\frac{1}{2\zeta_p^4}\sum_{i=1}^{N_\Phi}\sum_{j=1}^{N_\Phi}H_{i,j}^p q_i(t)q_j(t), \tag{14}$$

$$\ddot{q}_s(t)+\omega_s^2 q_s(t)=F_s(t)+\frac{1}{M_s}\sum_{k=1}^{N_\Phi}\sum_{n=1}^{N_\Psi}E_{k,n}^s q_k(t)\beta_n(t), \tag{15}$$

with $M_s = \int_S \rho h \Phi_s \Phi_s dS$ the modal masses, $F_s = \frac{1}{M_s} \int_S p \Phi_s dS$ modal force, and the coupling coefficients:

$$H^p_{i,j} = \int_S \Psi_p L(\Phi_i, \Phi_j) dS, \tag{16}$$

and

$$E^s_{k,l} = \int_S L(\Phi_k, \Psi_l) \Phi_s dS. \tag{17}$$

3.3 Linear modes

Due to the variable thickness, the solution to the eigenproblems (9-10) is particularly difficult and needs a dedicated numerical approach. The solutions are obtained using a finite difference method [4]. The use of an uniform grid for a structure where the wavelength varies spatially can result in a high computational cost. This problem is solved using a grid adapted to the flexural wavelength variation. The coefficients $H^p_{i,j}$ and $E^s_{k,l}$ are computed with the expressions (16, 17) from the numerical mode shapes, following the general procedure also described in [13] for finite element shell models.

3.4 Damping

The damping in the system is taken into account by assuming a small modal damping in the eigenvalue problem in displacement. The dissipative problem is written using a complex bending stiffness:

$$D^*(x) = D(x)(1 + \mathrm{j}\eta(x)), \tag{18}$$

where $\eta(x)$ is an equivalent loss factor obtained using the Ross-Ungar-Kerwin [4, 14] law for modeling the viscoelastic layer effect. The resolution of this new eigenvalue problem gives the modal loss factors ξ_s that are then directly used in the system (14-15), which finally reads:

$$\beta_p(t) = -\frac{S_w^2}{2\zeta_p^4 S_F} \sum_{i=1}^{N_\Phi} \sum_{j=1}^{N_\Phi} H^p_{i,j} q_i(t) q_j(t), \tag{19}$$

$$\ddot{q}_s(t) + 2\xi_s \omega_s \dot{q}_s(t) + \omega_s^2 q_s(t) = F_s(t) + \frac{S_F}{M_s} \sum_{k=1}^{N_\Phi} \sum_{n=1}^{N_\Psi} E^s_{k,n} q_k(t) \beta_n(t). \tag{20}$$

This method is advantageous since it yields a dissipative time evolution problem that can be solved in the same manner as for the conservative one. Secondly, it has been decided to include modal damping factor only on Eq. (20) for the transverse motions w. Neglecting possible losses in Eq. (19) can be more easily justified because inertia effects are not taken into account for the in-plane motions.

3.5 Time integration

The system of Eq. (19-20) is solved using a conservative integration scheme described in [12], that is conditionally stable. The first step is to discretize the modal coefficients $q_s(t)$:

$$q_s(t) \to q_s^n, \tag{21}$$

where $t = n\Delta t$ with Δt time step, and the derivation operators with finite difference operators. The conservative scheme then writes:

$$\delta_{tt} q_s^n + 2\xi_s \omega_s \delta_{t\cdot} q_s^n + \omega_s^2 q_s^n = \frac{S_F}{M_s} \sum_{k=1}^{N_\Phi} \sum_{l=1}^{N_\Psi} E^s_{k,l} q_k^n [\mu_{t\cdot} \beta_l^n] + F_s^n, \tag{22}$$

$$\mu_{t-} \beta_p^n = \frac{-S_w^2}{2\zeta_p^4 S_F} \sum_{i=1}^{N_\Phi} \sum_{j=1}^{N_\Phi} H^p_{i,j} q_i^n [e_{t-} q_j^n], \tag{23}$$

with the following discrete operators:

$$\delta_{tt}q^n = \frac{q^{n+1} - 2q^n + q^{n-1}}{\Delta t^2}, \tag{24}$$

$$\delta_{t.}q^n = \frac{q^{n+1} - q^{n-1}}{2\Delta t}, \tag{25}$$

$$\mu_{t-}q^n = \frac{q^n + q^{n-1}}{2}, \tag{26}$$

$$\mu_{t.}q^n = \frac{q^{n+1} + q^{n-1}}{2}. \tag{27}$$

$$e_{t-}q^n = q^{n-1}. \tag{28}$$

The stability condition of such a scheme is [12]:

$$f_e > \pi f_{\max}, \tag{29}$$

where $f_e = 1/\Delta t$ is the sampling rate and $f_{\max}$ is the largest frequency retained in the modal truncation for the transverse motion w.

4. NUMERICAL RESULTS

4.1 Parameters

The model is used to simulate the responses of five beams, denoted A, B, C, D and E. Tab. 1 gathers the parameters shared by all the configurations Tab. 2 presents the specificity of each configuration (see the geometry on Fig. 3). Configuration A is a uniform beam. Configurations B and C are beams with an ABH profile, covered and non covered with a damping layer, respectively. Configurations D and E are ABH beams with an extension of constant thickness and their termination is partially (D) or totally (E) covered with the damping layer.

The beams are discretized with a 1000×100 grid and the number of modes taken into account in the computation is N_Φ=100 and N_Ψ=2000. A convergence study, not presented in this paper for the sake of conciseness, allows to conclude that only 500 in-plane modes actually contribute to the coupling coefficients and permits to reduce the computational cost of this study.

Geometry		Material	
L	1.5 m	E	70 GPa
b	20 mm	ρ	2700 kg.m^{-3}
h_0	5 mm	ν	0.3
h_t	50 μm	E_l	1 GPa
l_{ABH}	30 cm	ρ_l	1000 kg.m^{-3}
h_l	100 μm	η_l	0.4

Table 1: Common material and geometrical parameters.

Name	A	B	C	D	E
l_{add} (mm)	/	/	/	100	100
x_{l1} (mm)	/	0	/	100	0
x_{l2} (mm)	/	300	/	400	400

Table 2: Extension and damping layer lengths.

4.2 Nonlinear regimes

The simulated beams A and B are first subjected to a sine excitation of increasing amplitude between 0 and 20 N during 10 s. The frequency is arbitrarily chosen to be 111 Hz. The time-frequency spectrograms of the response at the excitation point (x_0=0.6 m, y_0=0.01 m) are plotted on Fig. 4. The uniform beam A responds linearly: the spectrum only contains the excitation frequency. This not the case for the ABH beam B, the spectrum of which containing a large number of odd harmonics. This is the signature of a nonlinear regime where the energy is transferred to the high frequency part of the spectrum thanks to the appearance of numerous harmonics.

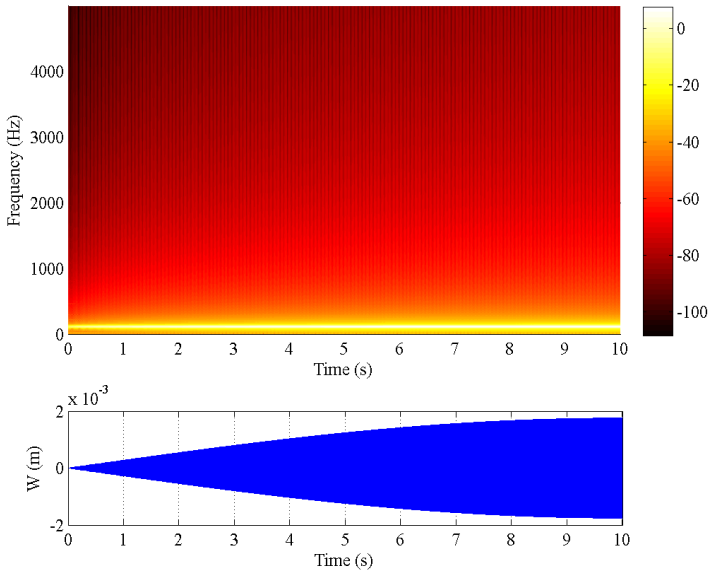

(a)

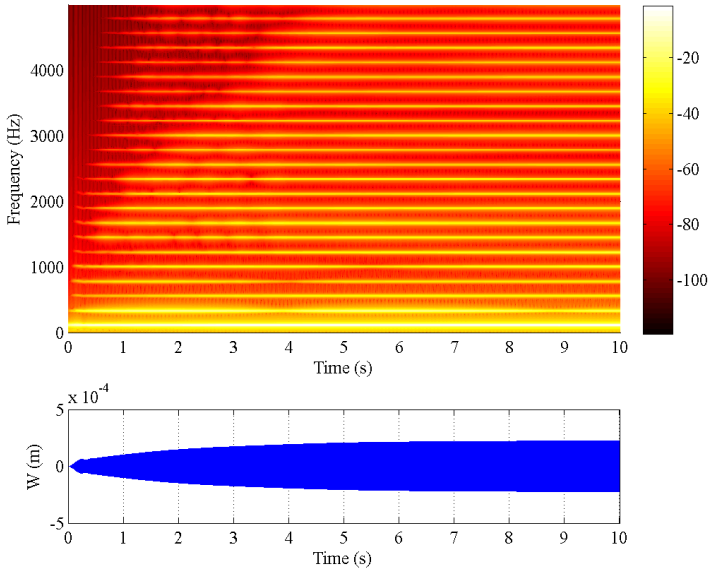

(b)

Figure 4: Spectrograms of the response to a sine at 111 Hz with increasing amplitude for configurations (a) A and (b) B.

4.3 Energy transfer

In order to observe the potential for an increased efficiency of the ABH in low frequency, the configurations A, B and C are excited with a white noise filtered on the 10-400 Hz range. Power density spectra of their response are displayed on Fig. 5 for several excitation amplitudes. The result for the uniform beam A (see Fig.5(a)) is as expected since the structure behaves linearly: the power is totally contained within the excitation range whatever the excitation amplitude. In the case of the covered ABH beam B, the response is linear for small amplitude but energy leaks toward high frequency when the amplitude increase (see Fig.5(b)). Even if the spectrum has a broadband content, the energy transfer is not sufficient for a significant reduction of the resonance peaks to be observed in the excitation band. However in the case of the non covered ABH beam C (see Fig.5(c)), the increase of amplitude of excitation allows for an efficient energy transfer and for a significant reduction of the resonances peaks at low frequency. The nonlinear effects tend to be so important here that a reduction is observed even without damping in the structure. In order to have more insight on these effects, two more configurations are simulated.

The constant thickness extension of configurations D and E is meant to increase the nonlinearities of the response. These beams are subjected to the filtered white noise excitation and results are presented on Fig. 6. Configuration D presents interesting results since the response is strongly nonlinear even for small amplitude excitations; for large amplitude excitation a significant reduction of the resonance peak can be observed. The equivalent added damping is due to nonlinear effects. When the same extension is fully covered (E), the response is linear (see Fig. 6(b)) which shows that an important damping tends to counteract the nonlinear effects, while the two phenomena were balanced in configuration D. More insight can be gained on these results by realizing a parametric study of the importance of the extension length and the damping layer characteristics.

5. CONCLUSIONS

In this paper, the nonlinear behaviour of ABH beams has been investigated. The experiment showed that the spectrum of the response of an ABH beam to a filtered white noise is not limited to the excitation range but is broadband, due to nonlinear effects and the large amplitudes of displacement of the small thickness region. The development of a numerical model of nonlinear von Kármán plate with variable thickness confirms the experimental observation. The nonlinearities allow to excite a broadband spectrum from a low frequency excitation. This phenomenon of energy transfer can be used to reduce the amplitude of the resonance peaks in low frequency and thus increase the efficiency of the ABH treatment. An extension of constant thickness can be added to the termination in order to increase the nonlinear effects while the damping layer tends to reduce these effects.

REFERENCES

[1] V.V. Krylov and F.J.B.S. Tilman. Acoustic 'black holes' for flexural waves as effective vibration dampers. *Journal of Sound and Vibration*, 274(3-5):605–619, 2004.

[2] V.B. Georgiev, J. Cuenca, F. Gautier, L. Simon, and V.V. Krylov. Damping of structural vibrations in beams and elliptical plates using the acoustic black hole effect. *Journal of Sound and Vibration*, 330(11):2497–2508, 2011.

[3] M.A. Mironov. Propagation of a flexural wave in a plate whose thickness decreases smoothly to zero in a finite interval. *Soviet Physics: Acoustics*, 34(3):318–319, 1988.

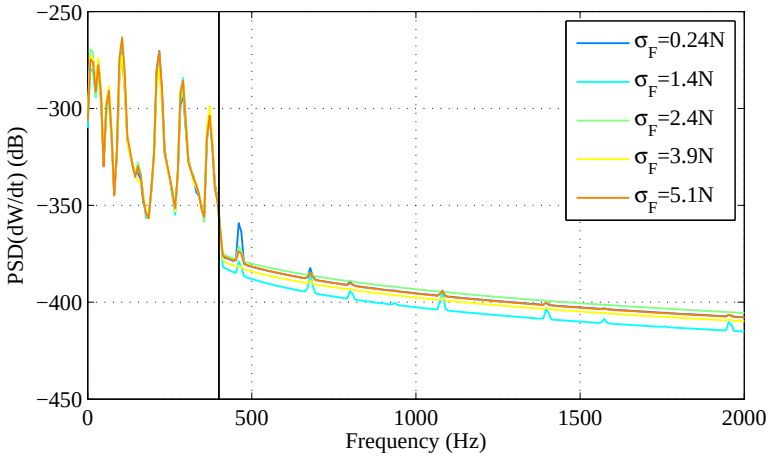

(a)

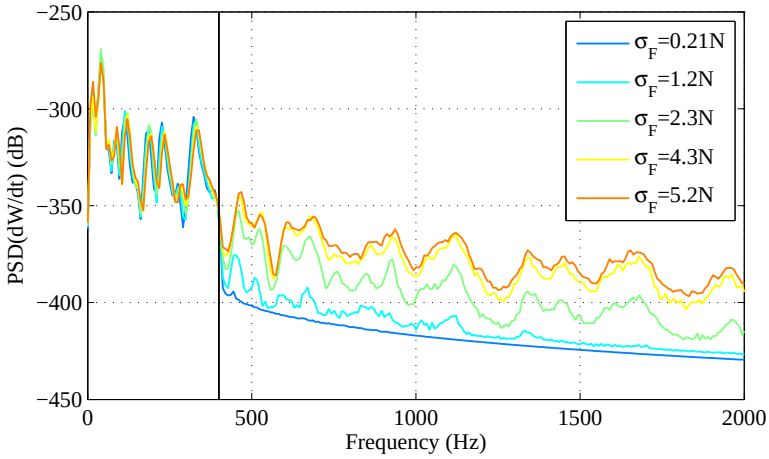

(b)

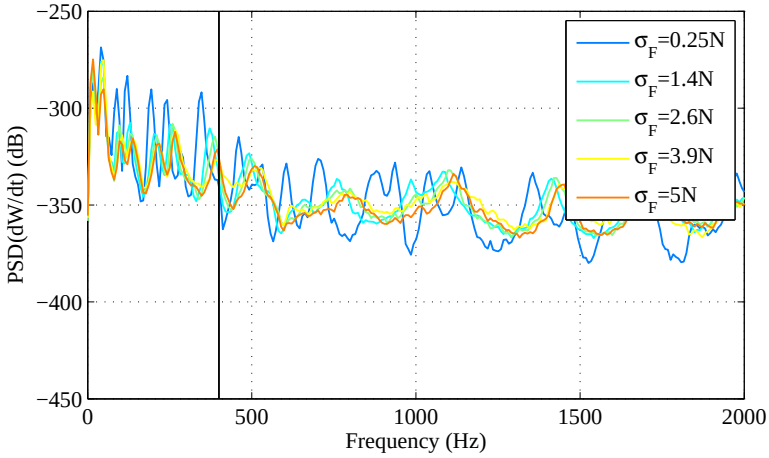

(c)

Figure 5: Power density spectrum of the response to a filtered white noise (10-400 Hz) excitation, normalized by the standard deviation of the force for configurations (a) A, (b) B and (c) C. σ_F denotes the standard deviation of the exciting force.

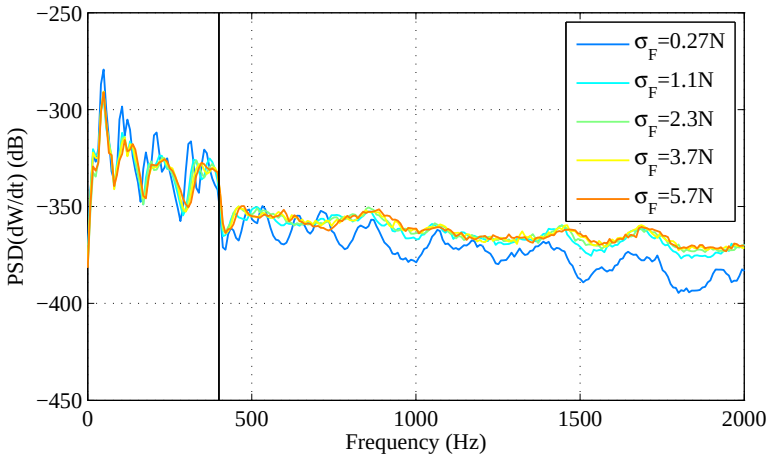

(a)

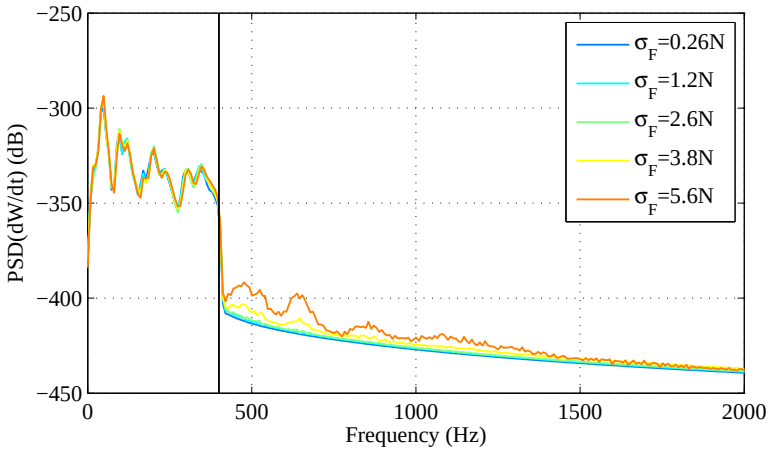

(b)

Figure 6: Power density spectrum of the response to a filtered white noise (10-400 Hz) excitation, normalized by the standard deviation of the force for configurations (a) D and (c) E. σ_F denotes the standard deviation of the exciting force.

[4] V. Denis, A. Pelat, F. Gautier, and B. Elie. Modal overlap factor of a beam with an acoustic black hole termination. *Journal of Sound and Vibration*, 333:2475–2488, 2014.

[5] D.J. O'Boy, V.V. Krylov, and V. Kralovic. Damping of flexural vibrations in rectangular plates using the acoustic black hole effect. *Journal of Sound and Vibration*, 329(22):4672–4688, 2010.

[6] E.P. Bowyer, D.J. O'Boy, V.V. Krylov, and J.L. Horner. Effect of geometrical and material imperfections on damping flexural vibrations in plates with attached wedges of power law profile. *Applied Acoustics*, 73(5):514–523, 2012.

[7] V. Denis, F. Gautier, A. Pelat, and J. Poittevin. Measurement and modelling of the reflection coefficient of an acoustic black hole termination. *Journal of Sound and Vibration*, 349:67–79, 2015.

[8] T. von Kármán. Festigkeitsprobleme im maschinenbau. *Enzyclopadie der Mathematischen Wissenschaften*, 4(4):311–385, 1910.

[9] A.H. Nayfeh and D.T. Mook. *Nonlinear oscillations*. Wiley New York, 1995.

[10] G.J. Efstathiades. A new approach to the large-deflection vibrations of imperfect circular disks using galerkin's procedure. *Journal of Sound and Vibration*, 16(2):231–253, 1971.

[11] O. Thomas and S. Bilbao. Geometrically nonlinear flexural vibrations of plates: In-plane boundary conditions and some symmetry properties. *Journal of Sound and Vibration*, 315(3):569–590, 2008.

[12] M. Ducceschi and C. Touzé. Modal approach for nonlinear vibrations of damped impact plates: application to sound synthesis of gongs and cymbals. *Journal of Sound and Vibration*, 344:313–331, 2015.

[13] C Touzé, M. Vidrascu, and D. Chapelle. Direct finite element computation of non-linear modal coupling coefficients for reduced-order shell models. *Computational Mechanics*, 54:567–580, 2014.

[14] D. Ross, E.L. Ungar, and E.M. Kerwin. Damping of plate flexural vibrations by means of viscoelastic laminae. In *Structural damping*, pages 49—57. J.E. Ruzicka, Oxford, Pergamon Press edition, 1960.